JMEPEG (2016) 25:2128–2137
DOI: 10.1007/s11665-016-2104-6

1059-9495/$19.00

Microstructure Modeling of a Ni-Fe-Based Superalloy During the Rotary Forging Process

A. Loyda, G.M. Hernández-Muñoz, L.A. Reyes, and P. Zambrano-Robledo

(Submitted February 2, 2016; in revised form April 14, 2016; published online May 11, 2016)

The microstructure evolution of Ni-Fe superalloys has a great influence on the mechanical behavior during service conditions. The rotary forging process offers an alternative to conventional bulk forming processes where the parts can be rotary forged with a fraction of the force commonly needed by conventional forging techniques. In this investigation, a numerical modeling of microstructure evolution for design and optimization of the hot forging operations has been used to manufacture a heat-resistant nickel-based superalloy. An Avrami model was implemented into finite element commercial platform DEFORM 3D to evaluate the average grain size and recrystallization during the rotary forging process. The simulations were carried out considering three initial temperatures, 980, 1000, and 1050 °C, to obtain the microstructure behavior after rotary forging. The final average grain size of one case was validated by comparing with results of previous experimental work of disk forging operation. This investigation was aimed to explore the influence of the rotary forging process on microstructure evolution in order to obtain a homogenous and refined grain size in the final component.

Keywords inconel 718 superalloy, microstructure, numerical modeling, rotary forging

1. Introduction

Nickel-based superalloys find extensive use in the hottest parts of aircraft engines. These superalloys constitute over 50% of the engine weight (Ref 1). The Inconel 718 superalloy, with service temperatures up to 650 °C, is one of the most important superalloys due to its physical and mechanical characteristics including high proof strength, tensile ductility, low creep extension, fracture toughness, and resistance to crack propagation (Ref 2, 3). The main components made of Inconel 718 superalloy are turbine blades for steam and gas turbines, structural parts for aerospace industry, turbine disks of engine mounts for aircrafts (Ref 3). Controlling the grain size is of great importance to fulfill the requirements of manufactured components.

At present most of the industrial forging companies are geared towards the production of parts by conventional bulk forming techniques. Conventional forging is a well-established route for the production of many components. This factor coupled with the knowledge and expertise gained in conventional bulk forming has created a reluctance to change to novel processes (Ref 4). The superalloys are more difficult to forge than most metals due to their strength retention at elevated temperatures. The forgeability varies widely depending on the type of superalloy and its exact composition (Ref 1).

Advanced metal forming process such as rotary forging has some benefits compared with the conventional forging processes, for example, lower level of noise and vibration, uniform quality, smooth surface, close tolerance, and considerable savings in energy and materials cost. Owing to these significant advantages, rotary forging has been an attractive process in different fields such as aeronautic and automobile industry (Ref 5).

Rotary forging is an incremental forming process; the constant rotation movement together with the vertical translation of the conical upper die (with an inclination angle) compresses the workpiece incrementally rotating together with the lower die. Under the action of the two dies, the workpiece produces the incremental plastic deformation. It occurs easily in the contact area of the top surface, but not so easily in the bottom, because of the partial loading exerted on the workpiece top by a rotary upper die with a conical surface along the rotary direction (Ref 6). From top to bottom, the material area under stress increases gradually so that the absolute values of the stresses in various directions decrease, and then the main plastic deformation area minifies from top to bottom. In the middle of the contact area, the radial elongation is the first principal strain; however, in most of the plastic area, the tangential elongation plays the main role because of the rolling effect of a rotary die with a conical surface (Ref 7). Finally, at the end of the rotary forging process, the diameter of the top surface is bigger than that of the bottom, so that the shape of the workpiece is like that of a mushroom (Ref 8), and then the tangential strain in the top surface is much greater than that in the bottom.

Rotary forging can reduce the forming forces and obtain higher deformation ratios without cracks in one-step operation (Ref 9). Even some rotary forging machines can forge using up to 10 times less force than conventional forge equipment (Ref 4). The main parameters influencing the grain size during the

A. Loyda, G.M. Hernández-Muñoz, L.A. Reyes, and **P. Zambrano-Robledo**, Universidad Autónoma de Nuevo León, UANL, Facultad de Ingeniería Mecánica y Eléctrica, FIME, Ave. Universidad S/N, Cd. Universitaria, C.P. 66451 San Nicolás de Los Garza, NL, Mexico and Universidad Autónoma de Nuevo León, UANL, Centro de Investigación e Innovación en Ingeniería Aeronáutica, CIIIA, Aeropuerto Internacional del Norte, Carr. a Salinas Victoria Km. 2.3, C.P. 66600 Apodaca, NL, Mexico. Contact e-mail: alejandro_loyd@hotmail.com.

rotary forging process are the heat transfer at the contact area and the friction between the dies and the workpiece (Ref 10). For Inconel 718 superalloy, rotary forging temperature should be between 900 and 1120 °C (Ref 11).

The influence of the rotary forging in the microstructure evolution has presented different effects compared to other processes. For that reason, the modeling and simulation of microstructure evolution is one of the most important ways to improve the quality of the final forging. Phenomenological models are widely used in the simulation of the forging processes of metals and alloys. The common features of phenomenological models are that the recrystallized fraction and grain size can be expressed as functions of the process parameters (strain, strain rate, and temperature) to consider the effects of these forming parameters on the microstructural evolution of metals and alloys (Ref 12, 13).

During the hot forming of superalloys, material flow behavior is often very complex, and the control of microstructure is of great importance to optimize the final mechanical properties (Ref 14). The control of the variables of precision components from initial workpiece to the final forging is critical for the generation of consistent mechanical properties. In order to accurately simulate hot forming process by means of numerical techniques, such as finite element method, it is important to precisely understand the flow behavior. The formulation applied to predict recrystallization of Inconel 718 superalloy during the rotary forging process was the Johnson-Mehl-Avrami-Kolmogrov (JMAK) model, typically known as Avrami model (Ref 15). This mathematical model has been used extensively to model the flow behavior and microstructure evolution of steels for industrial applications (Ref 16).

This article focuses on modeling the characteristic changes in grain size associated with the production of Ni-Fe-based superalloys disks. With the high-temperature properties of forging superalloys being highly sensitive to the resultant grain structures. The ability to engineer the structure enables further optimization of the structural component. Coarse grain microstructure can be utilized to minimize creep deformation at the gas turbine disk; while refinement of the grains of the finished disk increases the resistance to fatigue crack growth/initiation and also provides a significant degree of Hall-Petch strengthening (Ref 17). Therefore, the objective of present study is to achieve a fine homogeneous grain size distribution in the final geometry and to analyze the recrystallization mechanism during the rotary forging process. The microstructure model was implemented into a commercial finite element platform DEFORM 3D. According to the microstructure evolving during the rotary forging, the relationship between the temperature and the grain size is analyzed to select the best condition in which a fine grain microstructure is obtained. The predicted results were compared with experimental results presented previously.

Table 1 Chemical composition of Inconel 718 superalloy (wt.%) (Ref 19)

Ni	Cr	Fe	Nb	Mo	Ti	Al
Bal.	17.00	18.00	5.00	2.80	0.65	0.20

2. Experimental Procedure

The material of the workpiece used to forge a disk is a Ni-Fe superalloy commercially known as Inconel 718. A typical chemical composition is shown in Table 1. A viscoplastic material formulation coupled with a heat transfer formulation was used for the workpiece analysis. The typical flow stress of Inconel 718 shows a peak stress at critical strain. After the initial peak stress, the flow stress continuously decreases and reaches a steady stress (Ref 18). The Inconel 718 flow stress curves behavior at different temperatures obtained from previous tests (Ref 19) are shown in Fig. 1.

Rotary forging process consists of an upper die, a lower die and a forging geometry. The upper die (with a nutation angle θ) rotates ($\dot{\emptyset}$) around the angle axis ($\emptyset$) and generates downward translation motion ($\dot{v}$) along the die axis (V). The lower die has a rotation motion ($\dot{\psi}$) synchronously around the rotary die axis (V), sweeping the workpiece. These movements progressively deform the workpiece until a final shape is formed. Figure 2 shows the principal movements performed during the rotary forging process.

The processing parameters adopted were correlated with conventional process parameters for rotary forging so that the industrial processes may be suitably designed (Ref 20-24). The numerical model is established using the DEFORM 3D code, in which it is considered as the processing parameters and geometry dimension described in Table 2. However, the upper die and lower die temperatures were assumed to 150 and 500

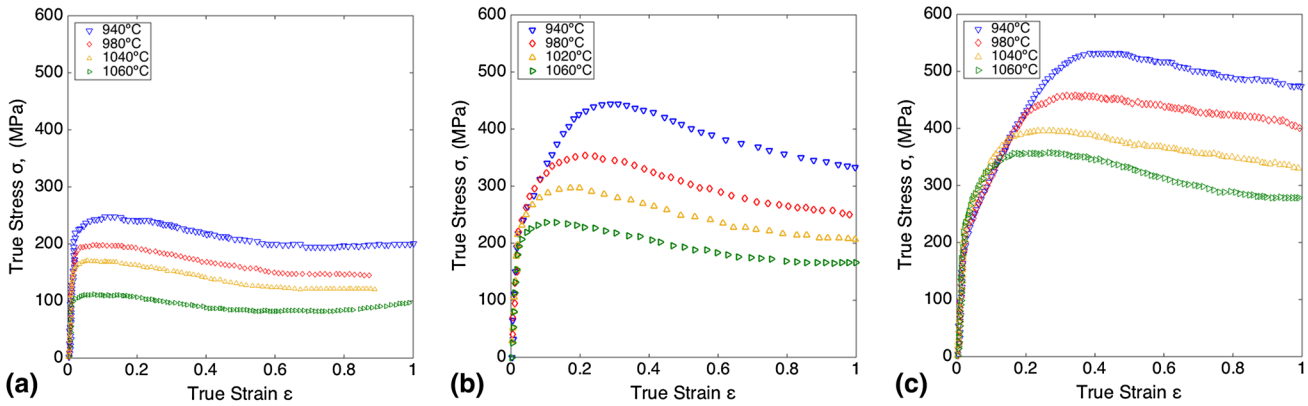

Fig. 1 The true stress-true strain curves of Inconel 718 at various strain rates: (a) $\dot{\varepsilon} = 0.01\ s^{-1}$; (b) $\dot{\varepsilon} = 0.1\ s^{-1}$; (c) $\dot{\varepsilon} = 1\ s^{-1}$ (Ref 19)

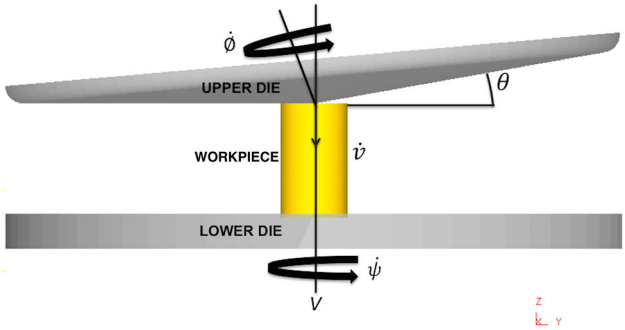

Fig. 2 Principal movements performed during the rotary forging process

Table 2 Parameters adopted in the simulation of the rotary forging process

Parameter	Value
Initial radius of workpiece (mm)	76
Initial height of workpiece (mm)	130
Radius of dies (mm)	800
Final height of the workpiece (mm)	30
Inclination angle of the upper die (°)	5
Rotational speed of the upper die (rpm)	300
Translational speed of the upper die (mm/s)	15
Rotational speed of the lower die (rpm)	300
Number of iterations	140

°C, respectively. The translational speed of the upper die was settled at 15 mm/s with a rotation speed of 300 rpm on both dies. The initial grain size was established as 15.9 μm and uniformly distributed in the workpiece.

The industrial forging conditions commonly control the grain size (Ref 24). Hence, in Inconel 718 δ phase presents an important role during hot deformation (Ref 25). Forging of Inconel 718 is performed at temperatures varying around 1000 °C at which some dispersed precipitates of δ phase limit grain growth (Ref 26). Below 940 °C, the γ' and γ'' precipitates harden the material, leading to excessive compression stresses during hot forging (Ref 25). The grain size of Inconel 718 depends highly on the presence of δ phase of which the solution temperature is around 1040 °C (Ref 27). Thus, the initial forging temperatures 980, 1000, and 1050 °C have been chosen for each simulation presented in this work to be near δ solvus temperature.

3. Numerical Modeling

A 3D finite element model of rotary forging is shown in Fig. 3. The dies are assumed as rigid bodies and the workpiece is assumed as plastic. The workpiece is discretized with tetra elements with 73,942 elements and 15,586 nodes. In the rotary forging process, the upper die continuously rotates around the angle axis, resulting in the frequent and rapid change in the contact condition, while the relative sliding may exist between the dies and workpiece during the rotary forging process (Ref 28). The mechanical properties of forgings are extremely sensitive to the thermomechanical variables (Ref 24). In order

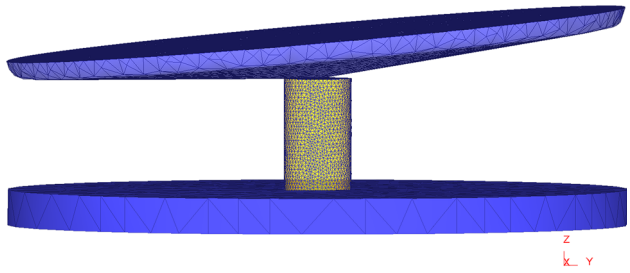

Fig. 3 Finite element model of the rotary forging process

Table 3 Materials property data used for FEM analysis of the rotary forging process

	Value
Thermal properties	
Convection coefficient (N/s/mm/C)	0.02
Thermal conductivity (N/(s °C))	26
Thermal expansion coefficient (°C)	1.86×10^{-5}
Emissivity	0.5
Mechanical properties	
Young's modulus (MPa)	202,706
Poisson's ratio	0.37

to achieve the desired properties of Inconel 718 superalloy forgings, mechanical properties were acquired from previous investigation of hot deformation behavior of Inconel 718 and used to optimize the thermomechanical processing parameters (Ref 2, 24), some details are given in Table 3. In order to lead an outward flow of the material, a low friction value was used, to represent the friction condition of the contact parts, based on previous experimental tests (Ref 29). In this model, a shear friction factor between dies and workpiece, m of 0.3 is adopted. However, the heat transfer coefficient at the contact between them was set to 11 N/s/mm/°C (Ref 30).

4. Microstructure Model

The phenomenological models combined with the FEM are carried out to investigate the rotary forging process. During hot forming process different microstructure changes can occur based on fundamental physical metallurgy principles: dynamic recrystallization (DRX), metadynamic recrystallization (MDRX), static recrystallization (SRX), and grain growth. Not all types of phenomena occur during a forging process (Ref 31). Depending on the combination of temperature, strain and strain rate, one recrystallization type or another can take place. The Avrami equation (Ref 32) is often used to evaluate the softening fractions induced by those phenomena. The general form of recrystallized fraction X of the Avrami equation as a function of time can be written as:

$$X = 1 - \exp(-kt^n). \quad \text{(Eq 1)}$$

The constants k and n depend on the material, temperature, previous strain history, and initial grain size. The coefficient n often called as the Avrami exponent varies between 2 and 5 depending on geometric considerations and the nucleation rate

(Ref 32). Specific Avrami expressions for dynamic, metadynamic, and SRX during thermomechanical processing are similar to Eq 1. The requirements for DRX to take place during the process in the Inconel 718 superalloy are temperature greater than 950 °C, deformation higher than a critical value and strain rate greater than 0.1 s^{-1}. Usually, the critical strain for the initiation of DRX can be expressed as a function of peak strain (ε_p). For the studied superalloy, the critical strain can be estimated as $\varepsilon_c = 0.80\varepsilon_p$ (Ref 14). In general, the basic characteristic of DRX kinetics is that there is an initial incubation period, then accelerates, and finally becomes steady (Ref 11). Usually, for Avrami equation the kinetics of DRX can be described by the following exponent type equation (Ref 33):

$$X_{drx} = 1 - \exp\left[-0.693\left(\frac{\varepsilon - \varepsilon_c}{\varepsilon_{0.5} - \varepsilon_c}\right)^n\right], \quad \text{(Eq 2)}$$

where X_{drx} is the volume fraction of DRX, ε is the applied strain, ε_c is the critical strain to span a nucleus and begin recrystallization, $\varepsilon_{0.5}$ is the strain for 50% volume fraction of DRX required at a specific temperature and strain rate for a given initial grain size to recrystallize half of the initial structure during deformation, n is the Avrami exponent. Dynamic recrystallized grain size (d_{drex}) was expressed as a function of Zener-Holloman parameter (Ref 14). The formulated equations for DRX are given in Table 4.

MDRX and SRX take place when deformation is higher than 80% of the critical value. Usually, MDRX completes the recrystallization process started and not finished by DRX (Ref 32). It occurs when the retained strain at the conclusion of deformation is greater than the critical strain. The volume fraction (X_{mrx}) and the grain size (d_{dmrx}) of meta-dynamic recrystallized grains also depend on initial grain size, accumulated strain, temperature, and strain rate. The kinetics of MDRX can be described by an Avrami equation as the following form:

$$X_{mrx} = 1 - \exp\left[-0.693\left(\frac{t}{t_{0.5}}\right)^n\right]. \quad \text{(Eq 3)}$$

MDRX time $t_{0.5}$ is defined as the holding time after deformation at which half of the starting structure has recrystallized (Ref 34). It depends on strain grade, deformation velocity, and dwell time after forging. Typically, MDRX grains are coarser than dynamically recrystallized grains. When the MDRX process is complete, any extended hold at elevated temperatures causes the grains to grow statically (Ref 35). The MDRX models constructed in the present study are tabulated in Table 4. SRX, will only occur if there has been sufficient accumulation of plastic strain ($\varepsilon > \varepsilon_{min}$) (Ref 34). The kinetics of SRX can be described by an Avrami equation of the following form:

$$X_{srx} = 1 - \exp\left[-0.693\left(\frac{t}{t_{0.5}}\right)^n\right]. \quad \text{(Eq 4)}$$

SRX kinetics is modeled similar to MDRX kinetics (Ref 32), where X_{srx} is the fraction of SRX (softening) fraction, n is the Avrami exponent, and $t_{0.5}$ is the time for the recrystalliza-

Table 4 Parameters of Avrami model for Inconel 718 superalloy (Ref 34, 35)

Description	Equation	Parameter
DRX kinetics	$X_{drx} = 1 - \exp\left[-0.693\left(\frac{\varepsilon - a_{10}\varepsilon_p}{\varepsilon_{0.5}}\right)^{k_d}\right]$	k_d= 2; a_{10} = 0.8
Required strain	$\varepsilon_{0.5} = a_5 d_0^{h_5}\varepsilon^{n_5}\dot{\varepsilon}^{m_5}\exp(Q_5/RT) + c_5$	a_5 = 5.043e−09; h_5 = 0; n_5 = −1.42; m_5 = −0.408; Q_5 = 196,000; c_5 = 0
DRX grain size	$d_{drx} = a_8 d_0^{h_8}\varepsilon^{n_8}\dot{\varepsilon}^{m_8}\exp(Q_8/RT) + C_8$	a_8 = 4.85e10; h_8 = 0; n_8 = −0.4; m_8 = −0.028; Q_8 = −240,000; c_8 = 0
MDRX kinetics	$X_{mdrx} = 1 - \exp\left[-0.693\left(\frac{t}{t_{0.5}}\right)^{k_m}\right]$	k_m = 1
Time after deformation	$t_{0.5} = a_4 d^{h_4}\varepsilon^{n_4}\dot{\varepsilon}^{m_4}\exp(Q_4/RT)$	a_4 = 5.043e−09; h_8 = 0; n_4 = −1.42; m_4 = −0.408; Q_4 = 196,000
MDRX grain size	$d_{mrx} = a_7 d_0^{h_7}\varepsilon^{n_7}\dot{\varepsilon}^{m_7} exp(Q_7/RT) + C_7$	a_7 = 4.85e10; h_7 = 0; n_7 = −0.4; m_7 = −0.028; Q_7 = −240,000; c_7 = 0
SRX kinetics	$X_{srx} = 1 - \exp\left[-0.693\left(\frac{t}{t_{0.5}}\right)^{k_s}\right]$	k_s = 0.3
Time after deformation	$t_{0.5} = a_3 d^{h_3}\varepsilon^{n_3}\dot{\varepsilon}^{m_3} exp(Q_3/RT)$	a_3 = 3.16; h_3 = 0; n_3 = −0.73; m_3 = 0; Q_3 = 74,790
SRX grain size	$d_{srx} = a_6 d_0^{h_6}\varepsilon^{n_6}\dot{\varepsilon}^{m_6}\exp(Q_6/RT) + C_6$	a_6 = 678; h_6 = 0; n_6 = 0; m_6 = 0; Q_6 = −31,694; C_6 = 0
Grain growth	$d = \left(d_0^m + a_9 t\, exp\left(-\frac{Q_9}{RT}\right)\right)^{1/m}$	a_9 = 1.58e16; Q_9 = 390,753; m = 2

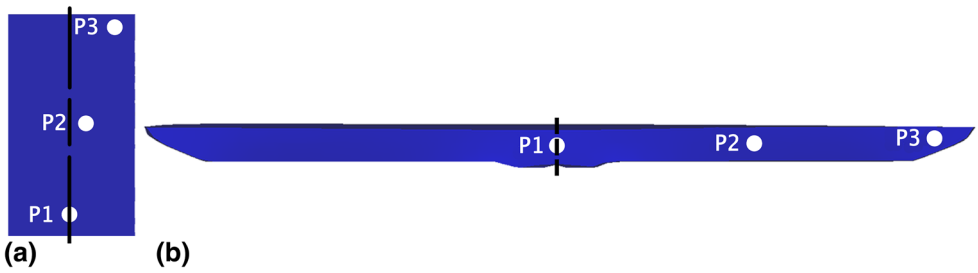

Fig. 4 Position of point sensors included in the numerical model of rotary forging; (a) at begin of the process, (b) at end of the process

tion volumetric fraction of 50%, the parameter used for this expression has been constructed in Table 4. For SRX, the grain size depends on the degree of strain and the initial grain size (Ref 12).

Under high-temperature deformation conditions, grain growth happens rapidly after recrystallization is completed and air cooling, which is related not only to holding temperature and time, but also to the grain size immediately after deformation (Ref 36, 37). The classical phenomenological grain growth relation is employed:

$$d_g = d_0^m + \text{atexp}\left(\frac{-Q}{RT}\right)^{1/m}, \quad \text{(Eq 5)}$$

where d is the grain size after deformation, t is the holding time and n is the material constant. The equations and its parameters used in the present study for recrystallization phenomena that take place during the rotary forging are tabulated in Table 4. For the microstructure simulation, user-defined subroutines, which include the previous phenomenological models, were implemented into the commercial platform DEFORM 3D. An average grain size was considered according to the evaluation of initial grain size. In addition, a recrystallized fraction of 0.5 was defined for initial microstructure computations.

5. Results

The aim of this section is to describe the influence of the initial temperature of workpiece on the microstructure evolution during the rotary forging. The simulation results were obtained from three point sensors included in the numerical model; these sensors are moving together with the geometry while it is deformed. Figure 4 shows the position of sensors in the geometry; point 1 is located at the central region, point 2 in the middle region and point 3 in the edge region. The variables analyzed were the temperature and the average grain size evolution during the rotary forging process.

The temperature during the rotary forging process has been plotted in Fig. 5 for each initial condition according to the point sensors defined. During forging the workpiece presents an increase in temperature due to the plastic deformation. Temperature can increase around 60 °C for nickel-based superalloys forging operations (Ref 38). Figure 5 illustrates the variation of forging temperature at three different regions during the rotary forging process; there is a similar trend in region P1 and P2 with a constant increase of temperature reaching the highest inner temperature in the central region; this region is greatly affected by the movement of the upper die with inclination angle, causing a greater plastic deformation. On another hand, the region P3 presents an increase in the temperature until certain value, then it is maintained constant during the rest of the process, under this condition the edge region goes away from the upper die, losing contact with the central region. However, at 1050 °C (Fig. 5c), there is a drop in temperature in region P3; this case presents the highest value even near the range of processing causing a no-uniform distribution (Ref 11).

Figure 6 shows the temperature distribution at the end of the rotary forging process. At 980 °C (Fig. 6a), was achieved a

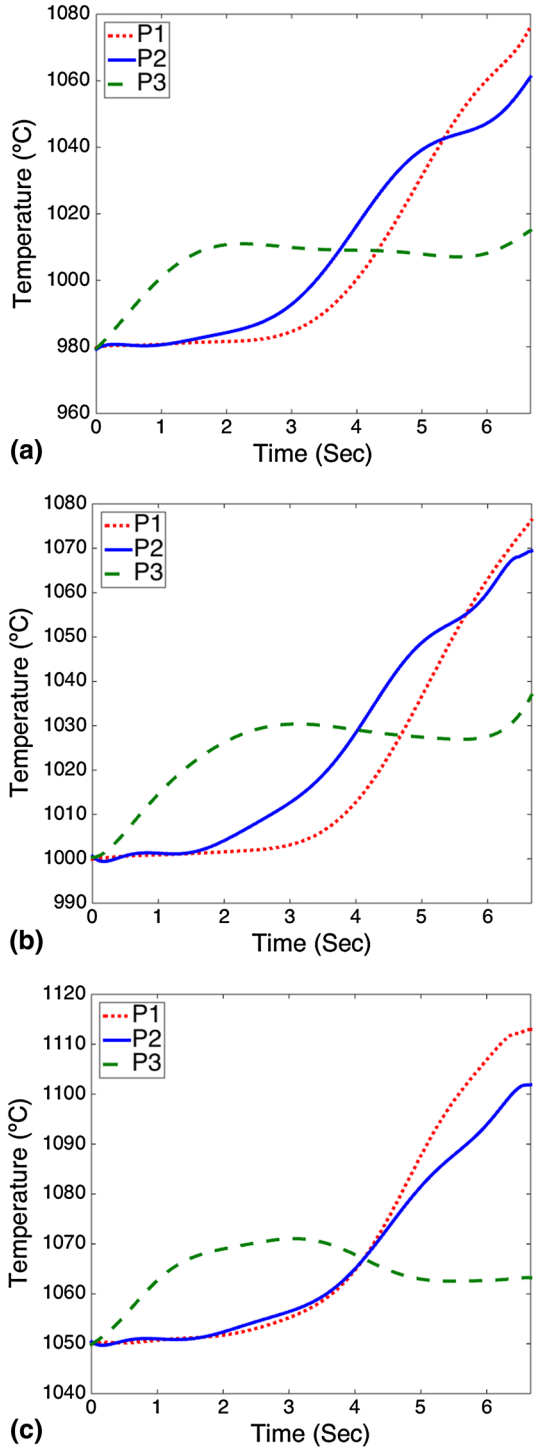

Fig. 5 Temperature evolution during the rotary forging process; (a) 980 °C, (b) 1000 °C, and (c) 1050 °C

better homogenous temperature distribution, even in the inner of the workpiece. While at 1050 °C, (Fig. 6c) there is a greater increase in the inner temperature as previously mentioned, due to the effect of the upper die in the top surface caused by the friction generated for its rotational and translational movements in the contact area, increasing the temperature to maintain similar to the lower surface which remains constant, because the lower die has a higher temperature. The effect of the temperature of dies was compared with previous work (Ref 20),

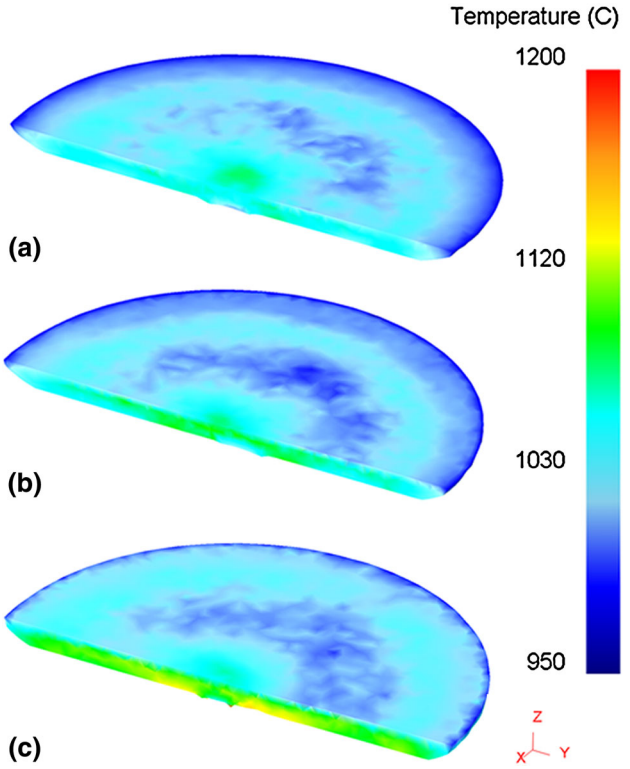

Fig. 6 Temperature distribution at the end of rotary forging process; (a) 980 °C, (b) 1000 °C, and (c) 1050 °C

where the optimal temperature of both dies was defined as 500 °C. However, the temperature distribution presented a greater difference between the minimum to maximum value.

The average grain size was analyzed to understand the relationship between the process variables and the temperature evolution. A higher increase in the temperature can cause an accelerated grain growth. The grain growth increases the grain size generated during recrystallization at temperatures higher than δ solvus temperature. The variation of the grain size for each initial temperature is shown in Fig. 7. Due the influence of rotary forging in the first second of the process, the recrystallization occurred with a refinement of microstructure for each condition, because the initial temperature is greater than 950 °C. At 980 °C (Fig. 7a) and 1000 °C (Fig. 7b), they were achieved a homogeneous microstructure avoiding the grain growth caused by δ solvus temperature; the grain size gradually decreases during the rotary forging; at P1 and P2, they decrease slowly suffering a high strain while at P3 decrease sharply suffering a low strain, this is the axial and radial deformation increase, and the recrystallization behavior in rotary forging is strongly affected by the degree of accumulative strain. Finally, at 1050 °C (Fig. 7c) the average grain size increased in P3 at the end of the process. This region was the first affected by the heat transfer of the upper die maintaining a temperature above δ solvus during all the processes.

The average grain size in the middle section of the final part after forging process and air cooling period is shown in Fig. 8. During air cooling, grain growth took place mainly for the overall volume of the workpiece. The grain size increased rapidly at the beginning of the cooling period. Then, the grain size reached a certain value at a different temperature

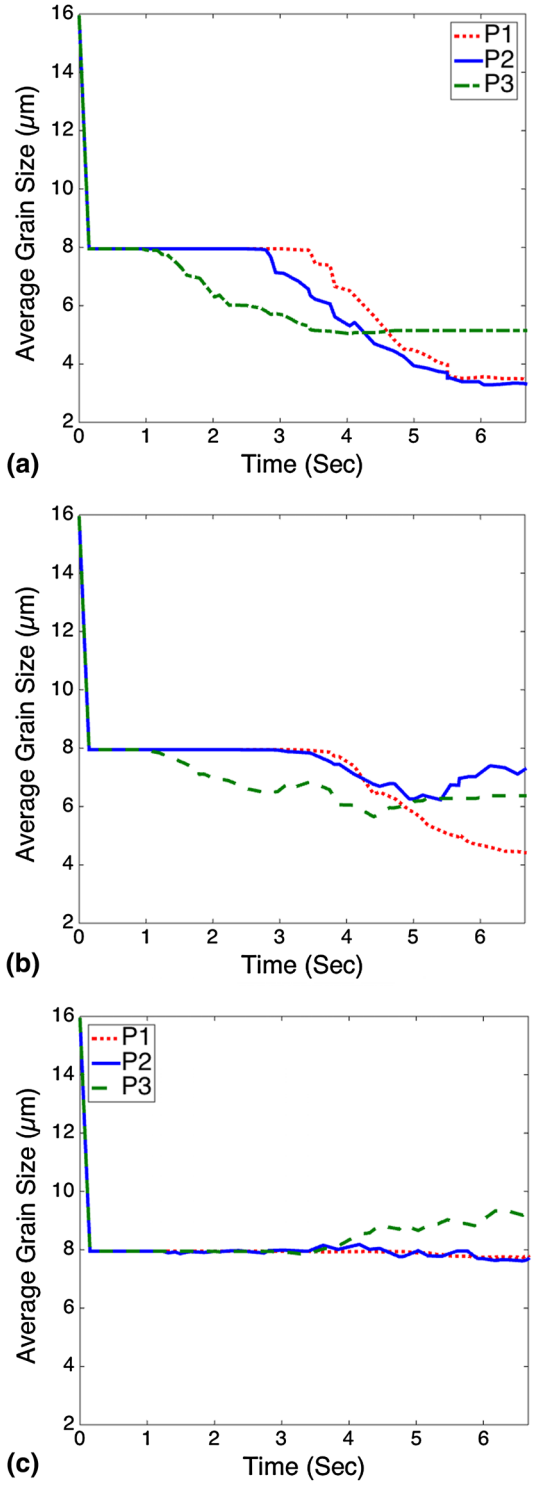

Fig. 7 Average grain size during the rotary forging process; (a) 980 °C, (b) 1000 °C, and (c) 1050 °C

(approximately 695 °C) growing slowly with further cooling time. The three regions are clearly distinguished by grain size distribution after air cooling for 30 min. The three models present a similar effect; all the regions were fully recrystallized during rotary forging process, presenting the smaller grain size in the edge region. The case at 980 °C (Fig. 8a) presented the better homogeneous distribution of grain size, achieving the smaller difference between minimum and maximum average

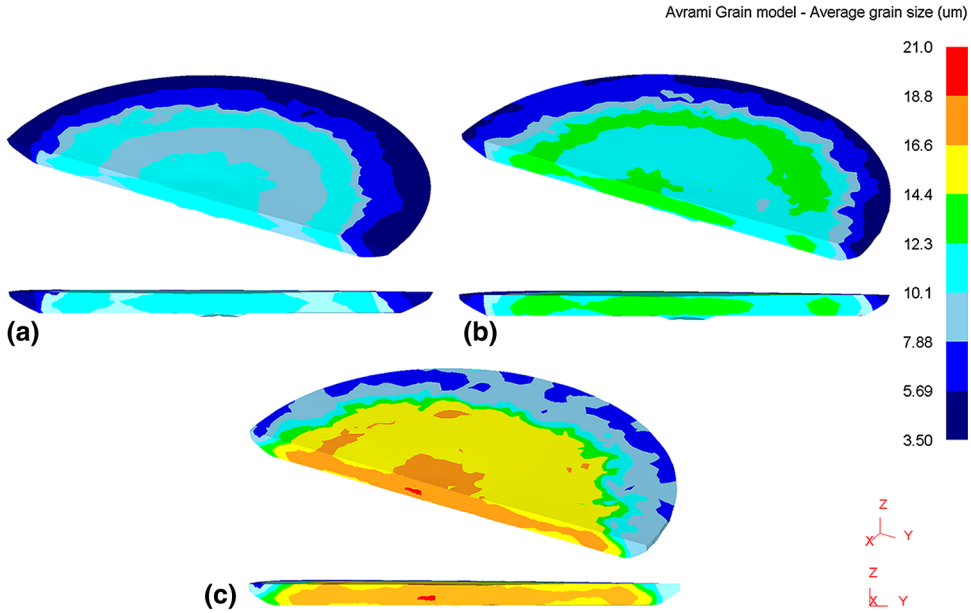

Fig. 8 Average grain size distribution after rotary forging process and cooling period; (a) 980 °C, (b) 1000 °C, and (c) 1050 °C

grain size, which are slightly larger than the grain size after deformation by forging process due the grain growth of the cooling period. The condition at 1000 °C (Fig. 8b) also presented fine grain size obtaining a homogenous distribution in central region at the end of the process. On the other hand, condition at 1050 °C (Fig. 8c) presented an increase in the grain size because its hot working was above δ solvus temperature from the beginning, reaching the highest temperature at the end of the rotary forging process. The final microstructure depends mainly on the grain size immediately after deformation. Therefore, in order to decrease the residual stress in the workpiece, air cooling should be employed, which will not cause the grain size to become too coarse (Ref 39).

To validate the microstructure evolution of the numerical model developed, a comparison with an experimental work is presented, selecting the case at 1000 °C, initial attention was focussed in experimental work of Mangas et al. (Ref 9), which was carried out with similar input data for the test: initial temperature of workpiece at 1000 °C, initial microstructure 11.2-15.9 µm, upper die temperature at 150 °C. Experimental and simulation results in each region studied are listed in Table 5. The forged sample after rotary forging and cooling period presents a similar behavior compared with the simulation results. The central region presented an average grain size more homogeneous than the edge region. Predicted average grain size values are in the same range of the experimental work. These results validate the previous section of the simulation model.

The strain rate is related with the process velocity of the dies; this variable also influences the final microstructure. Figure 9 shows the strain rate contour of the workpiece; it can be seen that the strain rate in the top surface is very complex; the region of the contact area as the part rotates is the most affected by the variation of the strain rate. Previously, it was demonstrated that reducing the process velocity caused a reduction of the strain rate, obtaining a heterogeneous microstructure mainly in the top surface in all the cases. Additionally, the workpiece presented greater heat loss. On the

Table 5 Comparison of measurements and predictions of the rotary forging process

Initial temperature of workpiece, °C	Region	Final average grain size (µm)	
		Experiment (Ref 9)	Simulation
1000	Central	13.3	13.25
	Middle	9	10
	Edge	4.7	5.69

other hand, the evolution of δ phase on DRX is sensitive to the deformation temperature and strain rate. The interfacial crack between the matrix and δ phase can cause flow instabilities under high strain rates. Meanwhile, δ phase precipitating at grain boundaries or within the grains can influence the hot working properties and fracture mechanisms of superalloys. The existence of δ phase can reduce the notch sensitivity of the material. However, too much δ phase will deteriorate the strength and plasticity of the material (Ref 14).

During processing of nickel-based superalloys, the recrystallization is a target of the forming process due to the lowering of the stress and nucleation of new grains with or without grain growth depending on the temperature, strain and time (Ref 20). The condition at 980 °C was selected to analyze the recrystallization behavior during the rotary forging process. DRX shows different behaviors above of δ solvus temperature acting as an obstacle against grain boundary movement.

In Fig. 10, the effective strain is observed at the end of the forging process. It can be seen that the highest strain appears at the center of the bottom surface, because the deformation of the bi-directional elongation and uni-directional compression occurs at the center continuously (Ref 21). Therefore, the strain becomes higher as deformation is accumulated. This condition has an average grain size of 6 µm in central region and an increase of recrystallized fraction. According to the Fig. 11, DRX fraction presents an increase for strain effective

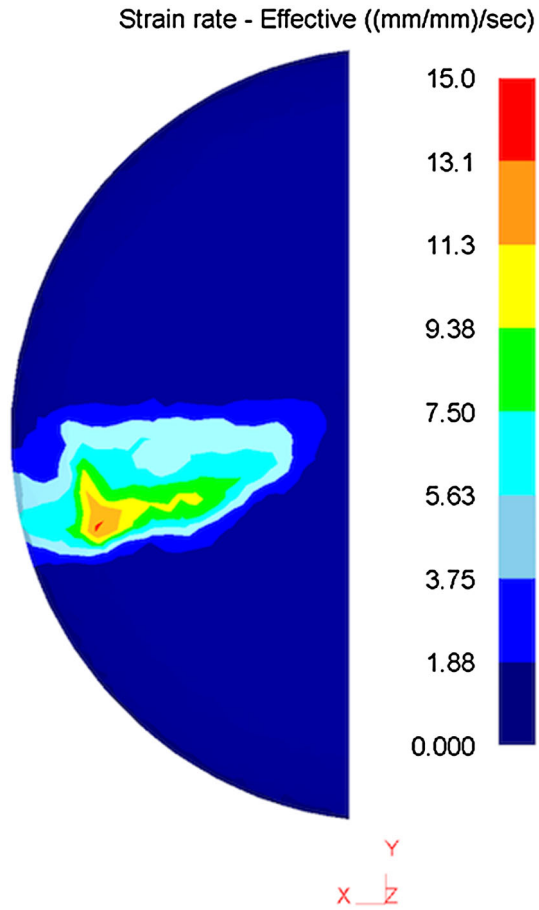

Fig. 9 Strain rate contour in the top surface of the workpiece

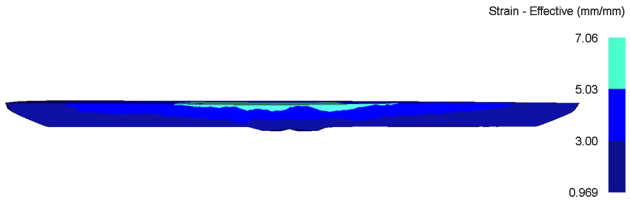

Fig. 10 Numerical results of effective strain at 980 °C

in the range of 3.00-5.03, reaching a maximum in the central region, while a minimum was observed in the edge region; this is because the material is tensioned in the tangential direction and compressed in the radial direction, hence has the lower value of stress than other regions. The deformation on the bottom surface is more difficult, due the effect of friction at the die-workpiece interface so that lower strain occurs in the lower region. Compared with Fig. 7 one can see that due to the low strain the grain size at the edge region decreased sharply achieving a lowest grain size than the central region that presented a large average of strain.

Figure 12 shows the dynamic recrystallized fraction as a function of effective strain in the three regions studied. The central and middle region were the most affected by the DRX due to the closeness with the nutation angle. When the upper die gets in contact with the workpiece area suffers a strain higher than the critical strain for DRX. The edge region was the less affected during the rotary forging process, because the

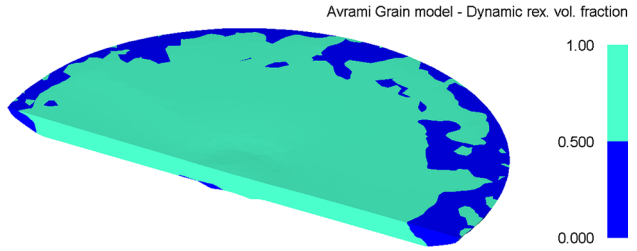

Fig. 11 Numerical results of dynamic recrystallized fraction at 980 °C

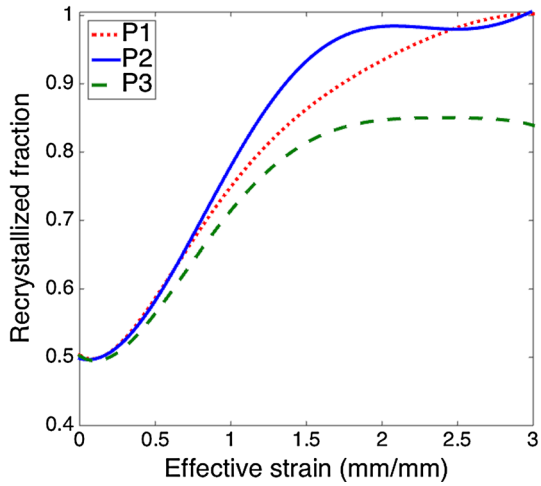

Fig. 12 Dynamic recrystallized fraction in selected points at 980 °C

partial loading is exerted on the workpiece top, and plastic deformation occurs in the edge region alternately following the swing of rotary die, while plastic deformation occurs at the center smoothly. Generally, DRX is an effective method to refine the grain size and reduce the hot deformation resistance (Ref 14). During the rotary forging process, DRX is the primary phenomena acting. DRX occurred when the material was deformed by the action of the upper die, while MDRX and SRX had a minimum effect appearing mainly in the edge region with low values during the cooling period. This effect occurred to finish the recrystallization when DRX stops due the lack of deformation. The recrystallization phenomena results were similar to the presented in previous work (Ref 20, 40). For the multi-pass hot forming process, the MDRX and SRX present a greater effect.

6. Conclusions

The rotary forging of an Inconel 718 superalloy was successfully simulated using a commercial finite element platform. The grain size of the rotary forged specimens has a great dependence on the initial temperature, strain rate, effective strain, and recrystallized fraction. Some conclusions can be drawn from the present study:

(1) The phenomenological models representing the effect of the DRX, MDRX, SRX, and grain growth on the Incon-

el 718 superalloy are implemented into finite element code, and the coupling between thermomechanical and microstructure evolution is realized. The central and middle regions are primary affected by the DRX due to the closeness with the nutation angle. In edge region, a partial loading is exerted on the workpiece top, and plastic deformation occurs alternately following the swing of rotary die.

(2) The grain size drops as the strain increases, and grain growth takes place during air cooling period. The final grain size depends mainly on the variation of the grain size immediately after deformation. However, air cooling will not cause grain size to become too coarse.

(3) The influence of initial temperature of workpiece on the grain size was analyzed through the rotary forging process simulation. At the beginning of the process a refinement is presented. The initial temperature at 980 °C achieves a homogenous microstructure at the end of the cooling period compared with conditions at 1000 and 1050 °C. The predicted grain sizes were compared with the experimental results. The comparison results have been successfully validated; the phenomenological and FEM models are reliable to predict the deformation behavior and microstructure evolution of the Inconel 718 superalloy during the rotary forging process.

(4) The variation of the temperature of dies has been analyzed. The lower die requires a higher temperature than the upper die to maintain a similar temperature in both surface of the workpiece during the process, due to the effect of friction produced by the rotational and translation movement of the upper die in the contact area while it operates, increasing the temperature of the upper region in the workpiece. The results of this study provide a better understanding of the influence of forging temperature on the grain size evolution of a rotary forged turbine disk.

Acknowledgments

The authors wish to thank the Programa para el Desarrollo Profesional Docente (PROMEP) for the financial support of the PROMEP DSA/103.5/14/10813 project; ''Modelación numérica de las propiedades físicas y mecánicas de anillos en aleaciones níquel cromo aplicados en investigaciones aeronáuticas.''

References

1. F. Campbell, *Manufacturing Technology for Aerospace Structural Materials*, Elsevier, Amsterdam, 2006
2. M. Perrais, A. Burteau, A. Seror, D. Poquillon, and E. Andrieu, Strain Rate and Temperature Effects on Crack Initiation of Direct Aged 718 Alloy, *MATEC Web Conf.*, 2014, **14**, p 16005
3. D. Huber, C. Sommitsch, and M. Stockinger, Comparison Between Microstructure Evolution in IN718 and ATI, Allvac® 718PlusTM—Simulation and Trial Forgings, *Adv. Mater. Res.*, 2011, **278**, p 168–173
4. A. Kocańda, *Development of Orbital Forging Processes by Using Marciniak Rocking-Die Solutions, 60 Excellent Inventions in Metal Forming*, Springer, Berlin, 2015, p 319–324
5. X. Han, L. Hua, W. Zhuang, and X. Zhang, Process Design and Control in Cold Rotary Forging of Non-rotary Gear Parts, *J. Mater. Process. Technol.*, 2014, **214**(11), p 2402–2416
6. G. Liu, S.J. Yuan, Z.R. Wang, and D.C. Zhou, Explanation of the Mushroom Effect in the Rotary Forging of a Cylinder, *J. Mater. Process. Technol.*, 2014, **151**(1), p 178–182
7. X. Han and L. Hua, Comparison Between Cold Rotary Forging and Conventional Forging, *J. Mech. Sci. Technol.*, 2009, **23**(10), p 2668–2678
8. Z. Decheng, Y. Shijian, Z.R. Wang, and X. Zhenrui, Defects Caused in Forming Process of Rotary Forged Parts and Their Preventive Methods, *J. Mater. Process. Technol.*, 1992, **32**(1), p 471–479
9. Á. Mangas, M. Santos, J.I. Zarazua, J. San José, G. Atxaga, and O. Adarraga, Sensitivity Analysis to Optimise the Microstructural Properties of an Inconel 718 Component Manufactured by Rotary Forging, *Key Eng. Mater.*, 2013, **554**, p 234–247
10. B. Buchner, A. Weber, and B. Buchmayr, Investigation of Friction in Warm Forging of AA6082, *Int. J. Mater. Form.*, 2008, **1**(1), p 1215–1218
11. D. U. Furrer, and S. L. Semiatin, Forging of Nickel-Base Alloys. ASM Handbook: A Metalworking: Bulk Forming, Vol 14, 2005, p 324–330
12. F. Chen, F. Ren, J. Chen, Z. Cui, and H. Ou, Microstructural Modeling and Numerical Simulation of Multi-Physical Fields for Martensitic Stainless Steel During Hot Forging Process of Turbine Blade, *Int. J. Adv. Manuf. Technol.*, 2016, **82**(1–4), p 85–98
13. F. Chen, Z. Cui, and J. Chen, Prediction of Microstructural Evolution During Hot Forging, *Manuf. Rev.*, 2014, **1**, p 6
14. X. Chen, Y. Lin, D. Wen, J. Zhang, and M. He, Dynamic Recrystallization Behavior of a Typical Nickel-Based Superalloy During Hot Deformation, *Mater. Des.*, 2014, **57**, p 568–577
15. A. Rollett, F.J. Humphreys, G.S. Rohrer, and M. Hatherly, *Recrystallization and Related Annealing Phenomena*, Elsevier, Amsterdam, 2004
16. H.W. Lee, S.H. Kang, and Y. Lee, Prediction of Microstructure Evolution During Hot Forging Using Grain Aggregate Model for Dynamic Recrystallization, *Int. J. Precis. Eng. Manuf.*, 2014, **15**(6), p 1055–1062
17. A. Kermanpur, P.D. Lee, M. McLean, and S. Tin, Integrated Modeling for the Manufacture of Aerospace Discs: Grain Structure Evolution, *JOM*, 2004, **56**(3), p 72–78
18. S.C. Medeiros, Y.V.R.K. Prasad, W.G. Frazier, and R. Srinivasan, Microstructural Modeling of Metadynamic Recrystallization in Hot Working of IN 718 Superalloy, *Mater. Sci. Eng. A*, 2000, **293**(1), p 198–207
19. F. Chen, J. Liu, H. Ou, B. Lu, Z. Cui, and H. Long, Flow Characteristics and Intrinsic Workability of IN718 Superalloy, *Mater. Sci. Eng. A*, 2015, **642**, p 279–287
20. Á. Mangas, M. Santos, J. San José, G. Atxaga, and O. Adarraga, Microstructural Behaviour in Rotary Forging of Inconel 718, *Key Eng. Mater.*, 2012, **504**, p 169–174
21. Z. Yu, Q. Ma, and Z. Lin, Simulation and Analysis of Microstructure Evolution of IN718 in Rotary Forgings by FEM, *J. Shanghai Jiaotong Univ.*, 2008, **13**(6), p 721–726
22. X. Han and L. Hua, Effect of Size of the Cylindrical Workpiece on the Cold Rotary-Forging Process, *Mater. Des.*, 2009, **30**(8), p 2802–2812
23. X. Han and L. Hua, 3D FE Modeling Simulation of Cold Rotary Forging of a Cylinder Workpiece, *Mater. Des.*, 2009, **30**(6), p 2133–2142
24. J. De Jaeger, D. Solas, O. Fandeur, J.H. Schmitt, and C. Rey, 3D Numerical Modeling of Dynamic Recrystallization Under Hot Working: Application to Inconel 718, *Mater. Sci. Eng. A*, 2015, **646**, p 33–44
25. S.H. Zhang, H.Y. Zhang, and M. Cheng, Tensile Deformation and Fracture Characteristics of Delta-Processed Inconel 718 Alloy at Elevated Temperature, *Mater. Sci. Eng. A*, 2011, **528**, p 6253–6258
26. A. Niang, B. Viguier, and J. Lacaze, Some Features of Anisothermal Solid-State Transformations in Alloy 718, *Mater. Charact.*, 2011, **61**, p 525–534
27. J. De Jaeger, D. Solas, T. Baudin, O. Fandeur and J.H. Schmitt, Inconel 718 Single and Multipass Modelling of Hot Forging, *Superalloys 2012*, E.S. Huron, R.C. Reed, M.C. Hardy, M.J. Mills, R.E. montero, P.D. Portella, J.Telesman, Ed., Wiley, p 663–672, 2012, TMS (The Minera, metal& material society)
28. X. Han and L. Hua, 3D FE Modeling of Cold Rotary Forging of a Ring Workpiece, *J. Mater. Process. Technol.*, 2009, **209**(12–13), p 5353–5362
29. X. Deng, L. Hua, and X. Han, Numerical and Experimental Investigation of Cold Rotary Forging of a 20CrMnTi Alloy Spur Bevel Gear, *Mater. Des.*, 2011, **32**(3), p 1376–1389

30. L. Filice, D. Umbrello, F. Micari and L. Settineri, On the finite element simulation of thermal phenomena in machining processes, *Advanced Methods in Material Forming*, Springer, Berlin, 2007, p 263–278
31. K. Subramanian and H.P. Cherukuri, Prediction of Microstructure Evolution During Multi-Stand Shape Rolling Of Nickel-Base Superalloys, *Integr. Mater. Manuf. Innov.*, 2014, **3**(1), p 1–24
32. J.P. Thomas, F. Montheillet, and S.L. Semiatin, Modeling of Microstructure Evolution During the Thermo-Mechanical Processing of Nickel-Base Superalloys, *ASM Handbook*, 2009, **22A**, p 566–582
33. C.M. Sellars, The Kinetics of Softening Processes During Hot Working of Austenite, *Czech J. Phys.*, 1985, **35**, p 239–248
34. D. Huang, W.T. Wu, D. Lambert and S.L. Semiatin, Computer Simulation of Microstructure Evolution During Hot Forging of Waspaloy and Nickel Alloy 718, Proceedings of Microstructure Modeling and Prediction During Thermomechanical Processing, R. Srinivasan, S.L. Semiatin, A. Beaudoin, S. Fox, Z. Jin, Eds., TMS, 2001, p 137–46
35. L. Reyes, P. Páramo, A. Salas, M. Zamarripa, M. de la Garza, and M. Guerrero-Mata MP, Influence of Processing Parameters on Grain Size Evolution of a Forged Superalloy, *J. Mater. Eng. Perform.*, 2015, **25**(1), p 179–187
36. G. Shen, J. Rollins, and D. Furrer, Microstructure modeling of forged waspaloy discs, *SUPERALLOYS 1996*, R.D. Kissinger, Ed., TMS, Warrendale, 1996, p 613–620
37. Q. Ma, Z.Q. Lin, and Z.Q. Yu, Prediction of Deformation Behavior and Microstructure Evolution in Heavy Forging by FEM, *Int. J. Adv. Manuf. Technol.*, 2009, **40**(3–4), p 253–260
38. Altan, G. Ngaile and G. Shen, Cold and hot forging: fundamentals and applications ASM Handbook 1, 2005, p 60–81
39. J.M. Zhang and Z.Y. Gao, Grain growth model of IN718 during holding period after hot deformation, *Mater. Sci. Eng. A*, 2000, **101**, p 25–30
40. J.P. Domblesky and R. Shivpuri, Grain Size Modeling and Optimization of Rotary Forged Alloy 718, *J. Eng. Mater. Technol.*, 1997, **119**(2), p 133–137